(*Abstract for the 34th International Workshop on Water Waves and Floating Bodies, Newcastle, Australia, 2019*)

# On the Four-wave Resonant Interactions in Finite Water Depth

Shuai Liu[*], Xinshu Zhang[†]

State Key Laboratory of Ocean Engineering, Shanghai Jiao Tong University, Shanghai 200240, China

Collaborative Innovation Center for Advanced Ship and Deep-Sea Exploration (CISSE) Shanghai, 200240, China

## 1 Introduction

Four-wave resonant interactions, including exact-resonant interactions and quasi-resonant interactions, play an important role in the energy transfers between different wave components for gravity waves. The fundamental theories for four-wave resonant interaction were first described in Phillips (1960) and Hesselmann (1962). Let $k_i$ denote the wave number for different wave component, and $\omega_i$ is the corresponding angular frequency. Once the waves fulfill the conditions, (i.e., $\mathbf{k_1} \pm \mathbf{k_2} \pm \mathbf{k_3} \pm \mathbf{k_4} = 0,\ \omega_1 \pm \omega_2 \pm \omega_3 \pm \omega_4 = 0$), resonant interaction occurs and energy transfer between these different wave components begins. Considering a special case with $\mathbf{k_1} = \mathbf{k_2}$, the resonant conditions reduce to $2\mathbf{k_1} - \mathbf{k_3} = \mathbf{k_4},\ 2\omega_1 - \omega_3 = \omega_4$, which mean that two mother waves (1) and (3) can give birth to a new resonant wave (4). The amplitude of new resonant wave is found to increase linearly with time, and the initial amplitude growth rate was studied by Longuet-Higgins (1962). Recently, in order to extend experimental validations of resonant interaction theory to more general waves, Bonnefoy *et al.* (2016) carried out a series of experiments with oblique mother waves crossing an acute angle. The results with respect to the growth rate and resonant curve are in quantitative agreement with the resonance theory.

However, few studies can be found on the four-wave resonant interactions in degenerate case for waves in finite water depth. Alternatively, another type of four-wave resonant interaction in case of modulation instability are extensively studied. In finite water depth, the wave-induced current is generated, which can subtract the energy for nonlinear focusing. As a consequence, with the decrease of water depth, nonlinear focusing process is suppressed, the modulation instability attenuates and eventually vanishes for sufficiently small water depth $k_0h < 1.36$ (where $k_0$ is the dominant wave number and $h$ is the water depth), as first found by Benjamin & Hasselmann (1967). However, this is valid for collinear perturbations, three-dimensional perturbations in finite water depth may still lead to modulation instability. Experimental observations with the support of numerical simulations devoted to the modulation instability of a plane wave to oblique perturbations in water of finite depth was discussed in Toffoli *et al.* (2013). It was observed that the carrier wave becomes unstable even for relative water depths $k_0h < 1.36$. Further, Fernandez *et al.* (2014) found that that modulation instability cannot sustain a substantial wave growth for $k_0h < 0.8$ through direct numerical simulations. For the degenerate case considered here, whether the generation of new daughter-wave will also eventually vanishes for sufficiently small water depth due to the effects of wave-induced current. Longuet-Higgins & Smith (1966) have proposed an approximate formulas by perturbation approach to consider the effect of water depth on wave resonant. However, it is rather limited owing to the assumption that the effect of water depth is small.

In present paper, direct numerical simulations are performed to investigate resonant interactions between two surface gravity waves in finite water depth in the degenerate case. Comparing to previous studies, the effects of water depth on the amplitude growth rate in the degenerated case are discussed. The mother-wave steepness and water depth are the control parameters. Considering the dynamical time scale of four-wave resonant interactions is about $T\epsilon^{-2}$ (where $T$ is the wave period and $\epsilon$ is the wave steepness), we also analyzed the evolution of growth rate for longer times rather than only the initial stage.

## 2 Four-wave resonant interaction theory

The fundamental theories of four-wave resonance were first established by Phillips (1960) and Hesselmann (1962) based on perturbation approach. Recently, Bonnefoy *et al.* (2016) investigated four-wave resonant interactions using Hamiltonian formulation to explain the detuning factor, where the results show good agreement with those using the classical theories. Here, based on these early studies, we report the resonant interaction theory.

The interactions between gravity waves completely satisfied the resonant condition are called as exact-resonant interactions. For deep water waves, the solutions were presented as the well-known figure-of-eight given by Phillips (1960). The expected wave amplitude of new resonant wave was shown by Longuet-Higgins (1962) to be given by

$$a_4^{res} = \epsilon_1^2 \epsilon_3 \cdot d \cdot G(\theta), \tag{1}$$

[*]Presenting author

[†]Corresponding author, Innovative Marine Hydrodynamics Lab at SJTU (xinshuz@sjtu.edu.cn)

Table 1: Input parameters of the resonant waves employed in the numerical simulations.

| Case | $k_1$ | $\epsilon_1$ | $\theta_1$ | $k_3$ | $\epsilon_3$ | $\theta_3$ | $\Delta\omega_l$ | $h$ |
|---|---|---|---|---|---|---|---|---|
| A | 3.2757 | $0.028, 0.041, 0.056$ | $12.5^\circ$ | 2.0500 | 0.050 | $-12.5^\circ$ | 0.0454 | 0.9 |
| B | 3.2757 | $0.028, 0.041, 0.056$ | $12.5^\circ$ | 2.0500 | 0.050 | $-12.5^\circ$ | 0.0755 | 0.7 |
| C | 3.2757 | $0.028, 0.041, 0.056$ | $12.5^\circ$ | 2.0500 | 0.050 | $-12.5^\circ$ | 0.0958 | 0.5 |

where $\epsilon_i$ is the wave steepness defined by $\epsilon_i = k_i a_i$, $a_i$ is the wave amplitude, $d$ denotes the distance from the wave maker and $G(\theta)$ denotes to the theoretical growth rate. It means that the daughter wave is expect to grow linearly with the distance to the wave maker. Bonnefoy *et al.* (2016) showed that the growth rate follows

$$G(\theta) = T_{1134}\frac{\omega_1}{k_1^3}\sqrt{\frac{\omega_3 k_4^2}{g\omega_4 k_3^3}}, \tag{2}$$

where $T_{1134}$ is the interaction kernel given in Krasitskii (1994). The theoretical and experimental results of growth rate $G(\theta)$ have been presented as a function of the angle $\theta$ in Bonnefoy *et al.* (2016). The growth rate reaches the maximum for $\theta = \theta_m = 25^\circ$ ($\gamma = \gamma_m = 1.258$). A relationship $d = c_g t$, where $c_g$ is the group velocity, is used to convert from temporal variation to spatial variation. In this study, the group velocity reduces to $\frac{1}{2}c_4$. The evolutions of wave phase have also been investigated. It is found that the phase of each wave component follows $2\varphi_1 - \varphi_3 - \varphi_4 = \frac{\pi}{2}$, where $\varphi_1$, $\varphi_2$ and $\varphi_4$ are the phase angle of each wave component, respectively.

Those results are about exact-resonant interactions, where the occurrence conditions are relatively strict. Apart from exact-resonant interactions, near-resonant interactions as an another kind of resonances, also play an important role in wave evolutions. The near-resonant conditions in degenerated case correspond to $2\mathbf{k_1} - \mathbf{k_3} = \mathbf{k_4}$, $2\omega_1 - \omega_3 = \omega_4 + \Delta\Omega$, where the detuning or mismatching factor is $\Delta\Omega \sim O(\epsilon^2)$. It consists of linear detuning $\Delta\omega_l$ and nonlinear detuning $\Delta\omega_n$, Besides, the correction for mutual interaction is also included (see detail in Longuet-Higgins (1962)). Based on perturbation approach it is derived that the amplitude of the daughter wave follows (also see Bonnefoy *et al.* (2016))

$$a_4 = a_4^{res}|\sin\frac{\Delta\Omega t}{2}| = \epsilon_1^2\epsilon_3 G(\theta)\frac{c_4}{\Delta\Omega}|\sin\frac{\Delta\Omega t}{2}| \tag{3}$$

The relationship between the phase of each wave component is

$$2\varphi_1 - \varphi_3 - \varphi_4 + \frac{\Delta\Omega t}{2} = \frac{\pi}{2} \tag{4}$$

When the effects of water depth are included, the dispersion relationship is different from the one for deep water waves. Hence, the resonant wave systems in deep water cannot satisfy the resonant conditions for finite water depth, whereas the near-resonant interactions are trigged.

# 3 Numerical results and discussion

Numerical simulations are performed by using a in-house code based on high order spectrum (HOS) method, which directly solves the field equation with the free surface boundary conditions in the Zakharov form (see Dommermuth & Yue (1987) and West *et al.* (1987)). The initial two mother waves are generated to give birth to a new resonant wave. The related input parameters are listed in Table 1, including the mother-wave wave number ($k_1$ and $k_3$) and wave steepness ($\epsilon_1$ and $\epsilon_3$) and propagation direction ($\theta_1$ and $\theta_3$), as well as the water depth $h$. Here, the angle $\theta = \theta_1 - \theta_3$ between two mother waves is fixed ($\theta = 25^\circ$) where the maximum growth rate of the daughter wave occurs. Wave direction for each mother wave are made symmetrical $\theta_1 = -\theta/2$ and $\theta_3 = -\theta/2$ to maximize the uniformity of the wave field. The wavenumbers $|\mathbf{k_1}|$ and $|\mathbf{k_3}|$ are determined according to the experiments in resonant conditions performed by Bonnefoy *et al.* (2016): $|\mathbf{k_1}| = 3.28, |\mathbf{k_2}| = 2.05$. Wave steepness for mother waves are chosen from low steepness to higher steepness: fixed $\epsilon_1 = 0.05$ and varied $\epsilon_2 = 0.028, 0.041, 0.056$. Three typical water depth $h = 0.5, 0.7, 0.9$ m are adopted with the scaled water depth corresponding to $k_1 h = 1.64, 2.29.2.95$.

The computation domain is a rectangle of $20\pi$ m$\times 40\pi$ m. Note that the resolution in wavenumber domain is determined by the length of the computation domain in $x$ direction $L_x$ and $y$ direction $L_y$: $\Delta k_x = 2\pi/L_x$ and $\Delta k_y = 2\pi/L_y$. A large number of nodes $512 \times 1024$ (before de-aliasing) were selected to capture the free surface elevation and velocity potential. The nonlinear order $M = 3$ is adopted to consider four-wave nonlinear interactions. 4th-order Runge-Kutta time integration with $\Delta t = T_1/50$ is used. The energy transfer between different scales due to four-wave resonant interaction for waves with a narrow range in frequencies and directions is over $T\epsilon^{-2}$. However, the classical resonance theory and later experimental and numerical validations focus on the initial stage. Here, the temporal evolutions for longer time are performed with numerical simulations, the total duration is set equal to $t = 100T_1$, where $T_1$ is the wave period of swell system.

A typical example of wave elevation and wavenumber spectrum at $t = 0$ sec and $t = 38.5$ sec (around $35T_1$) is shown in Fig. 1. Initially, the wave field consists of two mother waves $\mathbf{k_1}$ and $\mathbf{k_3}$, propagating in $12.5^\circ$

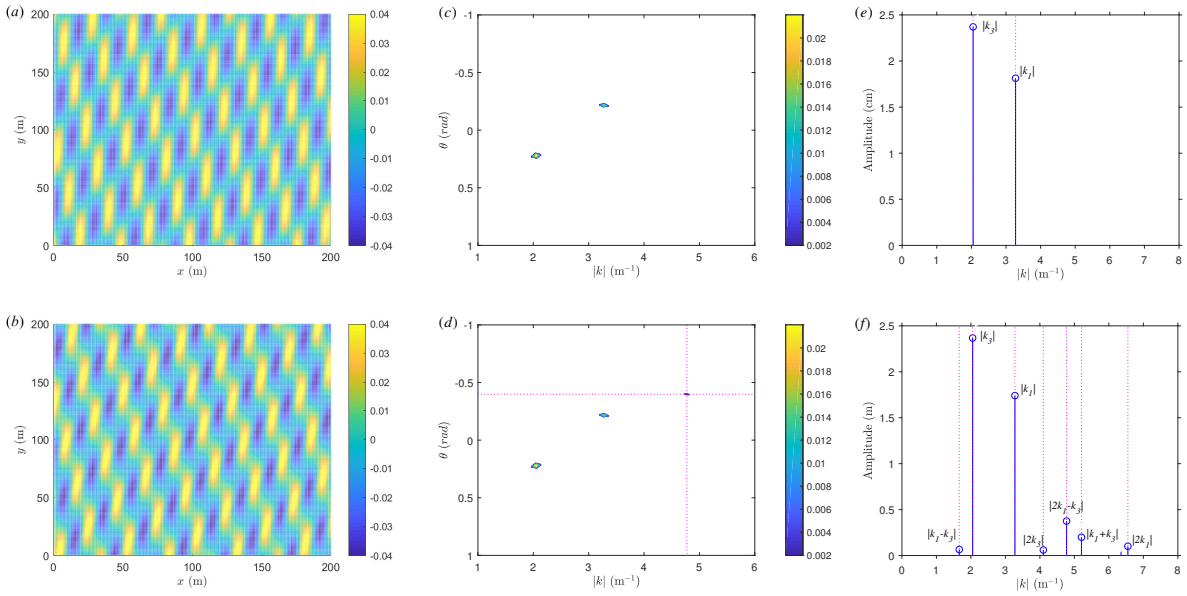


Figure 1: Example of surface elevation and wave spectrum of resonant wave system. $(a)(b)$ the surface wave elevation recorded at $t = 0$ sec and $t = 38.5$ sec. $(c)(d)$ The corresponding directional spectrum. $(e)(f)$ The corresponding omnidirectional spectrum. Vertical dotted lines correspond to wavenumbers: $|\mathbf{k_1} - \mathbf{k_3}|, |\mathbf{k_3}|, |\mathbf{k_1}|, |\mathbf{2k_3}|, |\mathbf{2k_1} - \mathbf{k_3}|, |\mathbf{k_1} + \mathbf{k_3}|, |\mathbf{2k_1}|$. Conditions $\theta = \theta_m, \epsilon_1 = 0.056, \epsilon_3 = 0.05, k_1 h = 2.95$.

and $-12.5°$ respectively. As expected, the initial crest lines shown in Fig. 1(a) are along the directions $77.5°$ and $102.5°$, which are perpendicular to the propagating directions of two mother waves. As waves evolve, the individual crest seem to be rotated clockwise slightly. A discrete fourier transform is applied to the surface elevations with a standard FFT algorithm, and the directional and omnidirectional spectrum are obtained. The peak at frequency $|\mathbf{2k_1} - \mathbf{k_3}|$ confirms the existence of the daughter wave, as expected, its amplitude is smaller than those of the mother waves. This is a first piece of evidence for a daughter wave generated by resonant interactions. Note that harmonics at frequency $\mathbf{2k_3}$, $\mathbf{2k_1}$, $\mathbf{k_1} + \mathbf{k_3}$ and $\mathbf{k_1} - \mathbf{k_3}$ are also visible, with amplitudes yet lower than that of the daughter wave. They are the signature of second-order bound waves accompanying the mother waves.

We also investigate the growth rate of of new resonant wave and phase locking of resonance wave system. For comparisons and validations, the numerical results for deep water waves with different steepness is presented. As shown in Fig. 2(a), at short times, the amplitude is found to grow linearly with time, which is in good agreement with the experimental observations by Bonnefoy *et al.* (2016) and theoretical results expected from Eqn. (1). Note that the experimental data have been transformed from spatial domain to temporal domain based on the group velocity. As the wave evolves, the amplitude growth is suppressed. Eventually, the daughter wave seems to reach a quasi-stationary stage. The evolution of interaction phase $\varphi = 2\varphi_1 - \varphi_3 - \varphi_4$ of the resonant wave system is shown in Fig. 2(b). It is found that, in the initial stage ($0 < t < 40$ sec) the interaction phase $\varphi$ is constant with time and equal to $\pi/2$. This phase locking phenomenon observed through our numerical simulations agrees well with the theoretical results and experimental observations by Bonnefoy *et al.* (2016). However, for longer times, the value of $\sin(\varphi)$ decreases with time.

When these three different resonant wave systems evolve in finite water depth, the exact-resonant conditions can not be satisfied and quasi-resonant interactions are trigged instead. We modelled their propagations in different water depth, respectively. A typical example of the temporal evolution of wave amplitude is presented in Fig. 3(a). To compare with resonance theory, the wave amplitude expected from Eqn. (3) is also shown after determining the detuning factors $\Delta\Omega$ (including linear detuning, nonlinear detuning, mutual interaction corrections) and growth rate $G(\theta)$ by Eqn. (2). It is suggested that the numerical results agree well with the theoretical predictions. The daughter-wave amplitude varies periodically, and the recurrence period tends to be significantly different in different water depth. The obtained maximum amplitude increases with wave steepness $\epsilon_1$. Fig. 3(b) shows the interaction phase $2\varphi_1 - \varphi_3 - \varphi_4$ as a function of time in finite water depth. For all the cases, the phase is locked at $\pi/2$ for a initial short time, which is in good agreement with theoretical results for near-resonant interactions expected from Eqn. (4). As waves evolve, the phase decreases rapidly to $-\pi/2$ ,and after staying constant for a time the phase increases to $\pi/2$ again. The variations of interaction phase tend to be periodic. The abrupt shift of phase (from $\pi/2$ to $-\pi/2$ or from $-\pi/2$ to $\pi/2$) is found to the be consistent with the moment when the daughter wave amplitude $a_4$ is very close to 0.

In this study, numerical simulations of the evolution of degenerated four-wave resonance wave system by HOS were performed to investigate the growth rate of daughter wave amplitude and phase locking phenomenon. Those properties for deep water waves have been studied experimentally by Bonnefoy *et al.* (2016). Here, we

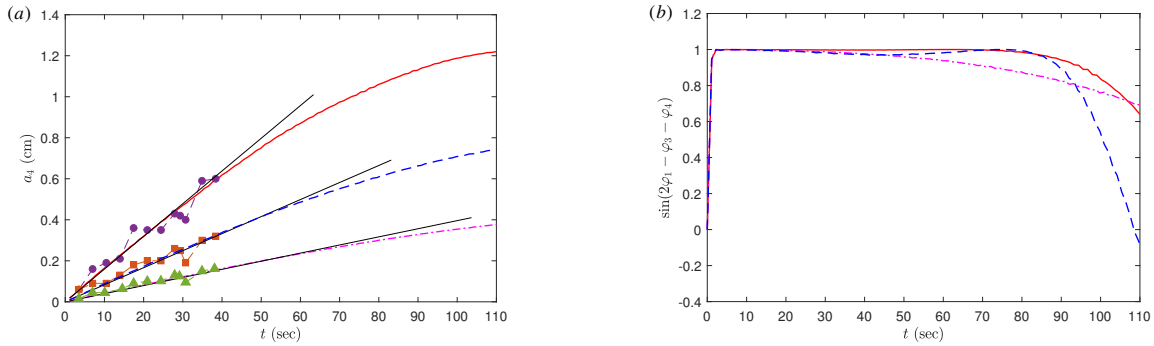


Figure 2: ($a$) Amplitude evolution of resonant wave $a_4$ in deep water for fixed $\theta = \theta_m$, $\epsilon_3 = 0.05$ and different $\epsilon_1 = 0.028, 0.041, 0.056$ (from bottom to top). For comparisons, the corresponding experimental results by Bonnefoy *et al.* (2016) are plotted in lines with markers and the theoretical results expected from Eqn. (1) are plotted in solid lines. Experimental data: $\epsilon_1 = 0.028$ (▲), $\epsilon_1 = 0.041$ (■), $\epsilon_1 = 0.056$ (●). ($b$) The evolution of interaction phase $2\varphi_1 - \varphi_3 - \varphi_4$ of the resonant wave system in deep water. $\epsilon_1 = 0.028$ ($- \cdot -$), $\epsilon_1 = 0.041$ ($- - -$), $\epsilon_1 = 0.056$ (——).

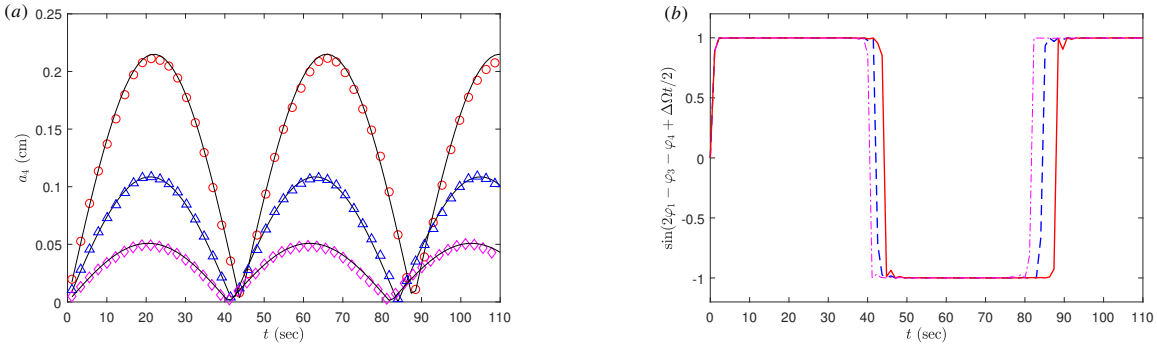


Figure 3: ($a$) The evolution of new resonant wave amplitude in finite water depth. $\epsilon_1 = 0.056$ (○), $\epsilon_1 = 0.041$ (△), $\epsilon_1 = 0.028$ (◇). The solid lines are theoretical results expected from Eqn. (3). ($b$) The interaction phase $2\varphi_1 - \varphi_3 - \varphi_4$ as a function of time. $\epsilon_1 = 0.028$ ($- \cdot -$), $\epsilon_1 = 0.041$ ($- - -$), $\epsilon_1 = 0.056$ (——). Conditions $\theta = \theta_m, \epsilon_3 = 0.05, k_1 h = 2.29$.

extended it to include the effect of water depth. Two mother waves with different initial steepness were generated in three different water depth ($k_1 h = 2.95, 2.29, 1.64$), as well as infinite water depth. For deep water waves, the results showed good agreement with theoretical and experimental results in initial stage. When those wave trains evolved in finite water depth, the detuning factor was introduced. The temporal evolutions of the amplitude of new resonant wave $a_4$ are shown to assume *sin* function, which is substantially distinct from the situation for deep water waves. The obtained wave amplitude evolutions are in good agreement with the resonance theory by Longuet-Higgins (1962) and Bonnefoy *et al.* (2016). With respect to the interaction phase $2\varphi_1 - \varphi_3 - \varphi_4$, the temporal evolutions are found to lock at $\pi/2$ initially, as waves evolve the phase value change with $\pi$ periodically. The abrupt change is found to the be consistent with the time when the daughter wave amplitude $a_4$ nil, which is distinct from the case in deep water. More comprehensive analyses and discussion will be presented in the workshop.

# References


Benjamin, S. J. & Hasselmann, K. 1967 *Proc. Roy. Soc.* **299** (299), 59–75.

Bonnefoy, F.and Haudin, F., Michel, G., Semin, B., Humbert, T., Aumaitre, S., Berhanu, M. & Falcon, E. 2016 *J. Fluid Mech.* **805**, R3.

Dommermuth, D. & Yue, D. K. P. 1987 *J. Fluid Mech.* **187**, 267–288.

Fernandez, L., Onorato, M., Monbaliu, J. & Toffoli, A. 2014 *Nat. Hazards Earth Syst. Sci.,* **14** (3), 705–711.

Hesselmann, K. 1962 *J. Fluid Mech.* **12(15)**, 481–500.

Krasitskii, V. 1994 *J. Fluid Mech.* **272**, 1–12.

Longuet-Higgins, M. S. 1962 *J. Fluid Mech.* **12**, 321–332.

Longuet-Higgins, M. S. & Smith, N. D. 1966 *J. Fluid Mech.* **25**, 417–435.

Phillips, O. M. 1960 *J. Fluid Mech.* **9**, 193–217.

Toffoli, A., Fernandez, L., Monbaliu, J., Benoit, M., Gagnaire-Renou, E., Lefvre, J. M., Cavaleri, L., Proment, D., Pakozdi, C. & Stansberg, C. T. 2013 *Phys. Fluids.* **25** (9), 204502–1057.

West, B. J., Brueckner, K. A. & Janda, R. S. 1987 *J. Geophys. Res.* **92** (11), 11803.